

Pretraining Billion-scale Geospatial Foundational Models on Frontier

Aristeidis Tsaris *

National Center for Computational Sciences
Oak Ridge National Laboratory
Oak Ridge, TN, USA

Philippe Ambrozio Dias

Geospatial Science and Human Security
Oak Ridge National Laboratory
Oak Ridge, TN, USA

Abhishek Potnis

Geospatial Science and Human Security
Oak Ridge National Laboratory
Oak Ridge, TN, USA

Junqi Yin

National Center for Computational Sciences
Oak Ridge National Laboratory
Oak Ridge, TN, USA

Feiyi Wang

National Center for Computational Sciences
Oak Ridge National Laboratory
Oak Ridge, TN, USA

Dalton Lunga

Geospatial Science and Human Security
Oak Ridge National Laboratory
Oak Ridge, TN, USA

Abstract—As AI workloads increase in scope, generalization capability becomes challenging for small task-specific models and their demand for large amounts of labeled training samples increases. On the contrary, Foundation Models (FMs) are trained with internet-scale unlabeled data via self-supervised learning and have been shown to adapt to various tasks with minimal fine-tuning. Although large FMs have demonstrated significant impact in natural language processing and computer vision, efforts toward FMs for geospatial applications have been restricted to smaller size models, as pretraining larger models requires very large computing resources equipped with state-of-the-art hardware accelerators. Current satellite constellations collect 100+TBs of data a day, resulting in images that are billions of pixels and multimodal in nature. Such geospatial data poses unique challenges opening up new opportunities to develop FMs. We investigate billion scale FMs and HPC training profiles for geospatial applications by pretraining on publicly available data. We studied from end-to-end the performance and impact in the solution by scaling the model size. Our larger 3B parameter size model achieves up to 30% improvement in top1 scene classification accuracy when comparing a 100M parameter model. Moreover, we detail performance experiments on the Frontier supercomputer, America’s first exascale system, where we study different model and data parallel approaches using PyTorch’s Fully Sharded Data Parallel library. Specifically, we study variants of the Vision Transformer architecture (ViT), conducting performance analysis for ViT models with size up to 15B parameters. By discussing throughput and performance bottlenecks under different parallelism configurations, we offer insights on how to leverage such leadership-class HPC resources when developing large models for geospatial imagery applications.

Index Terms—Foundation Models, Vision Transformers, Distributed Training, Remote Sensing, Geospatial

I. INTRODUCTION

Automated analysis of Earth Observation (EO) data using artificial intelligence (AI) tools is emerging as one of the cornerstones enabling fast and cheap exploitation of geospatial information to describe and assess physical features as well as geographically referenced events on Earth. EO data entails

capturing information about the Earth’s surface using sensors mounted on e.g. satellites and in-situ instruments. Deep neural network (DNN) models have significantly advanced the state of the art in automated analysis of remote sensing (RS) data, enabling extensive applications in human dynamics, precision agriculture, disaster management, humanitarian assistance, and national security.

New sensing modalities with complementary imaging characteristics are becoming operational, monitoring larger extents of the Earth’s surface with improved temporal cadence and finer spatial resolution. While this presents great potential for a wide variety of applications, the sheer volume and diversity of RS archives continues to stretch the limits of human analysts and existing AI tools. Similar to other AI application domains, deep learning models currently employed for EO data analysis are limited in that: (i) they are task-specific, with limited generalization to unseen (out of distribution) data; (ii) they heavily rely on large volumes of manually annotated data samples for model training, which implies on high costs for model development.

Foundation models (FMs) are a recent breakthrough with demonstrated potential to address such limitations [1]. FMs can be defined as large models (ranging from 10^8 to 10^{12} of parameters) usually trained through self-supervised learning (SSL) on large volumes of unlabeled data, such that they learn generalizable features that can then be adapted at lower-costs for a wide variety of downstream tasks. First demonstrated for natural language processing (NLP), FMs are extending their impacts in other domains such as computer vision, across a variety of data types. A common practice is to fine-tune pre-existing FMs to align with particular use cases, but in the context of geospatial tasks, the multifaceted characteristics of the data pose additional constraints. While some recent works on RS data analysis have exploited the concepts of SSL for model pretraining, such efforts have been restricted to smaller model sizes than the proportions characteristic of FMs [2]–[4].

Recent advancements towards developing state-of-art foundation models for computer vision and natural language

*Corresponding author: tsarisa@ornl.gov

processing tasks, have highlighted the need for substantial compute and memory for the research and development of large-scale foundation models. Florence [5], an FM for computer vision with 893 million parameters, was trained for 10 days on 512 NVIDIA A100 (40GB) GPUs. Contrastive Language-Image Pre-Training (CLIP) [6] required 12 days on 256 NVIDIA V100 GPUs for training its largest ViT-based configuration. The ALIGN: A Large-scale Image and Noisy-text embedding [7] model was trained on 1024 Cloud TPUv3 cores, while GATO [8] with its 1.2 billion parameters was trained on 16x16 Cloud TPUv3 cores.

Such demand for vast amounts of data and high performance computing (HPC) resources are key major barriers limiting progress on the development of FMs for geospatial data. Critically, beyond accessibility to computing resources, expertise and guidelines on how to effectively train FMs using data and model parallel approaches remains limited to few established organizations. This underscores the importance of developing training methodologies that can be harnessed by communities aiming to control the model, enhance its performance, and tailor it to address specific application needs.

Within this manuscript, we present performance assessments and initial appraisal of pretraining billion-scale FMs on geospatial data sets. Our primary contributions are as follows:

- We present a practical guide for training billion parameter size ViT models on HPC systems, using the newest Pytorch’s FSDP model sharding library. We provide image-per-second baselines for various size ViT models, and discuss compute and communication costs to consider in training FMs for geospatial application workloads.
- We share best practices and study bottlenecks on distributing ViT training on the Frontier HPC system while scaling to various size models. ViT has been the backbone of many vision and multi-modal foundational models.
- We demonstrate the benefits of training billion-scale models for geospatial data, with linear-probing experiments highlighting gains up to +30% on remote sensing imagery classification tasks across three independent datasets. This is the largest size model trained on geospatial applications.

II. BACKGROUND AND RELATED WORK

Model architectures. In contrast to hand-crafted features based methods, convolutional neural networks (CNNs) trained over large amounts of labeled data have enabled significant progress in computer vision as they learn to extract hierarchical features that better capture semantically meaningful patterns. The UNet [9] encoder-decoder architecture is a representative example as it has been widely adapted for pixel-level semantic segmentation tasks of remote sensing image applications. However, the local nature of the convolution operator limits its ability to capture long-range interaction in scenarios that require larger context.

Attention mechanisms have been explored to address such issues, with the notion of *self-attention* at the core of novel architectures such as the Transformer architecture [10] that

has become the main reference architecture behind modern large language models (LLMs). The Vision Transformer (ViT) [11] first extended the concept of attention-only architectures for image processing, with following studies revealing their increased performance with scale [12], [13]. ViTs have thus emerged as the core architecture developing FMs for computer vision applications.

In contrast to preceding deep learning paradigms, FMs have distinct characteristics with respect to: (i) *scale* and *scope*, in terms of model size as well as pretraining with internet-scale data volumes; (ii) extraordinary *transfer learning* capabilities with fewer labeled datasets on a wide range of downstream tasks.

Pretraining mechanisms. Self-supervised learning (SSL) at scale is a key ingredient enabling the success of FMs. By leveraging surrogate tasks as sources of supervision when no labels are available, SSL unlocks the potential of learning from unprecedentedly large unlabeled datasets for which manual labeling would be unfeasible. Two main approaches prevail for SSL of computer vision models. As exemplified by the SimCLR framework [14], contrastive learning schemes exploit correlated views of the same image constructed through augmentations (e.g., random cropping and color distortions). During training, the model is tasked to maximize feature similarity between pairs augmented from the same image, while minimizing similarity between examples originating from different images. Analogous to the masked language model used for training NLP models [15], the denoising concept of masked autoencoders (MAEs) [16] enforces the model to reconstruct pixels of masked image patches based on the remaining visible image patches - this approach has been demonstrated to yield models with strong generalization capabilities.

Foundation Models for Remote Sensing. While contrastive learning methods for natural images typically rely on artificial augmentation to construct positive pairs, in the remote sensing domain approaches can perform SSL by aligning representations extracted from different image acquisitions covering the same location but from different timestamps and/or sensors [17]. More recently, multiple strategies targeting FMs for RS have been introduced leveraging MAE to pretrain larger Transformer-based architectures. The SatMAE described in [2] uses MAE to pretrain a ViT-L using optical imagery from the Functional Map of the World (fMoW) dataset [18], demonstrating its applicability on land cover classification and building segmentation tasks. The concept of MAE-based pretraining of ViT for RS is likewise exploited in [4], which proposes the idea of rotated varied-size attention (RVSA) to enhance the robustness of ViTs to the variations in size and orientation characteristic of objects when captured in remote sensing imagery. Similarly, the RingMo framework [3] adopts masked modeling at pixel-level for model pretraining, with patches that are only partially masked as a mechanism targeting better reconstruction and characterization of smaller structures.

Crucially, all such works toward FM for RS data have been

restricted to models with less than 300M parameters. RVSA [4] and RingMo [3] perform pretraining on datasets containing millions of images, but are both restricted to models based on the “base“ configuration of ViT that is the order of $< 100M$ parameters. While the SatMAE [2] work includes ViT-Large architectures, the approximately 300M parameters of that architecture are still far smaller than the 1B+ models powering FMs for other computer vision application domains.

In addition to the model size scaling challenge, FMs for RS involves training over large corpus of data for them to learn non-trivial features that are generalizable to a variety of downstream tasks. The RVSA exploited the MillionAID dataset [19] for model pretraining. Introduced for image classification tasks, the MillionAID dataset contains over one million RS scenes from various sensors and resolutions, with image sizes ranging from 110×110 to $31k \times 31k$ pixels. The fMoW dataset [18] used by SatMAE [2] contains over 500k optical image patches collected from multiple sensors, while [3] reports experiments using a custom (not publicly-available) dataset containing over 2M images.

Distributed deep learning. It is becoming evident as RS workloads grow that the pretraining of FMs will continue to demand enormous compute power and time in addition to substantial data storage. Although technological advancements have resulted in widespread use of HPC systems with powerful compute capabilities and vast storage, it is not feasible to subscribe to the notion of unlimited compute and storage. Distributed optimization strategies are there sought after to enable the growing compute at scale needs. This paradigm seeks to accelerate model training to achieve higher throughput by leveraging efficient optimization techniques and high-performance computing.

Parallelization strategies have become essential when training large deep neural network models whose memory footprint exceeds the memory of a single GPU device. These strategies can be broadly categorized into: (i) conventional perspective that involves data and model parallelism; and (ii) modern perspective that involves intra-operator and inter-operator parallelization [20]. In this work we leverage the PyTorch’s native Fully Sharded Data Parallel (FSDP) strategy [21], which takes inspiration from the Zero Redundancy Optimizer [22] that was first implemented in DeepSpeed [23] and later had an improved version implemented in PyTorch.

Evaluation protocols for FMs. Since the main targeted capability of FMs is the ability to extract features that are easily generalizable to multiple downstream tasks, evaluation protocols adopted by related works [1]–[5] are often based on the concepts of fine-tuning and linear probing. By their nature, FMs are very large, such that fine-tuning fewer tasks-specific layers is preferable from the perspective of computational and labeled-data budgets. Fine-tuning configurations can range between updating all layers of the model during downstream specialization, freezing specific layers/blocks (e.g., the pre-trained backbone), to the linear probing configuration where all pretrained parameters are frozen and parameter updates are thus restricted only to a final classification layer appended to

the pretrained model.

Results are typically contrasted to baselines trained in fully supervised schemes for multiple tasks. Related works adapting FM models for the RS domain typically conduct the evaluation on three main tasks: image classification, object detection, and semantic segmentation.

III. EXPERIMENTAL SETUP

In this section we discuss the model architectures adopted for experimentation, the hardware characteristics of the Frontier supercomputer, and the different sharding strategies enabled by the PyTorch’s FSDP library.

A. Model Architecture Variants

Table I summarizes the different ViT variants explored in the remainder of this work. The ViT base (ViT-Base) and huge (ViT-Huge) variants follow the original vision Transformer paper [24], with the ViT-Base containing 87M parameters, an embedding size (*width*) of 768, 12 encoder layers (*depth*), 12 heads per self-attention layer, configured with input patches 16×16 pixels large. For the ViT-Huge model and all listed billion-scale models, we adopt instead input patches that are 14×14 pixels large as per [24] and related works.

For the pretraining we used the MAE architecture. As discussed in the original MAE work [16], the decoder architecture for the image reconstruction pretraining task can be flexibly designed, with the MAE decoder being responsible for only a small fraction of the overall compute (e.g., $< 10\%$ of FLOPS per token as compared to a ViT-L encoder). Results from [16] shows that a lightweight decoder with 8 Transformer blocks and a width of 512 is sufficient for pretraining of ViT models with strong capabilities for linear probing. We similarly adopt such default configuration to define the decoder of our MAE architectures for ViT pretraining, with a loss function based on the mean squared error (MSE) between model reconstruction and original image, for normalized pixel values of each masked patch.

We use the notation ViT- x B to denote our models with x billion parameters. Scaling studies in [11] note that it is most effective to scale all aspects (depth, width, MLP-width, and patch-size) by similar amounts, while [12] performs extensive simulations to define ViT variants of different sizes. Following those empirical guides and [13], which has trained the largest ViT available today (22B parameters), we increase the number of encoder layers and heads by gradually scaling the embedding size from 768 to 5040.

TABLE I
VISION TRANSFORMER (ViT) MODEL ARCHITECTURES
EXPLORED IN THIS WORK

Model	Width	Depth	MLP	Heads	Parameters [M]
ViT-Base	768	12	3072	12	87
ViT-Huge	1280	32	5120	16	635
ViT-1B	1536	32	6144	16	914
ViT-3B	2816	32	11264	32	3067
ViT-5B	1792	56	15360	16	5349
ViT-15B	5040	48	20160	48	14720

B. Hardware and Software

All our experiments were performed using the Frontier Supercomputer [25] at the Oak Ridge Leadership Computing Facility. Each Frontier node has a single 64-core AMD EPYC CPU, and four AMD Instinct MI250X GPU accelerators. The MI250X GPU is comprised of two Graphics Compute Dies (GCDs), connected with Infinity Fabric CPU-GPU, while the four MI250X GPUs are connected with Infinity Fabric GPU-GPU of 50GB/s. The system identifies each GCD independently, so from the application perspective it can be considered that each node has 8 GPUs, each with 64 GB of high-bandwidth memory. For simplicity we are going to use the term GPU when referring to a GCD. The nodes are connected via a Slingshot-11 interconnect with 100GB/s, to a total of 9408 nodes, making it the first true exascale machine. For the software stack, we used PyTorch 2.1, ROCm v5.4.0, MIOpen v2.19.0, RCCL v2.13.4 with libfabric v1.15.2 plugin.

C. Sharding Billion Scale Models

We used PyTorch’s Fully Sharded Data Parallel (FSDP) [21] distributed strategy in order to scale both the batch size and the model size. On one GPU, with our current software stack, we can fit up to a 3B parameter ViT model. Still, the compute workload from a 100M parameter model to a 3B parameter is drastically different, such that even for models that can fit on a single GPU it is worth studying if distributing the compute to multiple GPUs will be a good trade off for the extra communication cost.

Scaling the batch size is usually done by copying the model across ranks, and doing collective all-reduce operations during the backward pass for sharing the gradients. PyTorch’s distributed data parallel (DDP) module has been widely used in the past for this distributed strategy. The FSDP mode equivalent to DDP is called NO_SHARD, where parameters, gradients, and optimizer states are not sharded across ranks. Even though algorithmically the two approaches are the same, their implementations are different. Moreover, while most preexisting studies are based on NVIDIA GPUs, this work relies on AMD GPUs to handle a very diverse workload in terms of computation operations. Given such differences, in this work we study the impact of DDP vs FSDP-enabled sharding strategies for different model configurations.

We chose FSDP because it is the native solution of PyTorch for zero-redundancy parallelism, and as such it can be leveraged for different model architectures without depending on third party implementations. Since it benefits from PyTorch built-in support for both NVIDIA CUDA and AMD ROCm stacks, it is expected to be more system independent and less likely to change, compared to other frameworks. Compared to DeepSpeed, FSDP offers several modes in terms of sharding strategies and communication optimizations, which can benefit optimal usage of different hardware systems.

Sharding configurations. In addition to the NO_SHARD strategy, FSDP offers the FULL_SHARD, SHARD_GRAD_OP and HYBRID_SHARD. The FULL_SHARD has the highest communication overhead, but

produces the lowest memory footprint. It shards parameters, gradients and optimizer states across devices, offering the largest overlap between compute and communication. In contrast, the SHARD_GRAD_OP shards only gradients and optimizer states during computation, while the model parameters are sharded outside computation. In this sharded strategy, the communication is lighter than FULL_SHARD but the memory footprint is increased.

The HYBRID_SHARD offers the most flexibility, since it is a hybrid strategy between model shard and model replica. For example, we define a strategy named HYBRID_2GPUs which applies HYBRID_SHARD on a single Frontier node (i.e., 8 GPUs total) such that only the two closest GPUs perform model sharding. Let the term *sharding-group* refer to the number of GPUs across which model sharding occurs. For a single node with 8 GPUs, such HYBRID_2GPUs strategy implies on 4 sharding-groups, each with 2 GPUs. Between the two closest GPUs, all-gather and reduce-scatter communication would occur, while the model will be replicated four times with all-reduce communication enabled for sharing parameters.

Analogously, we define a HYBRID_8GPUs strategy that allows model sharding across all 8 GPUs of a single node. For example, using HYBRID_8GPUs on two nodes allows forming 2 sharding-groups, with data-parallel performed across nodes. This mode is ideal for medium size models that can fit on a single node, reducing the communication overhead by performing only all-reduce across nodes.

IV. PERFORMANCE EVALUATION: SCALING MODEL SIZE

In this section, we discuss the measured computational costs as we scale the ViT variants. Specifically, we report memory footprint as well as throughput by measuring images-per-second (*ips*) for the six ViT models described in Table I, while pursuing different FSDP-sharding strategies.

A. MAE Workload Bottlenecks

We start by scaling our models up to the ViT-3B size for MAE-based pretraining configurations, which is the largest MAE model we can fit with our current software stack on a single Frontier’s GPU. Figure 1 shows the pretraining workload with the ViT-3B backbone for *IO*, synthetic (*syn*), and real application time (*real*). *IO* corresponds to the case where the PyTorch dataloader is ran in isolation, while for the synthetic configuration we run the model on cached data. The FSDP NO_SHARD strategy was used to scale the batch size up to 64 nodes, with a local batch size of 32, while using four data loader workers per GPU rank.

From the comparison between *io* and *syn* curves we can see that even for one node the *IO* is faster than synthetic, with the difference between the two getting larger as we scale to 64 nodes. Therefore, we can conclude that even if we improved the *IO*, we would not see any benefit on the real application time, as it is compute and/or communication bound.

The *syn no comm* curve refers to synthetic runs without any communication from FSDP, with its comparison of

throughput against the *syn* configuration providing insights on the communication costs of the application. We see that the communication cost does increase as we scale, reaching around 22% for the 64 nodes runs. That indicates that while the application is closer to compute bound for smaller scale runs, communication costs take over as we increase the number of nodes.

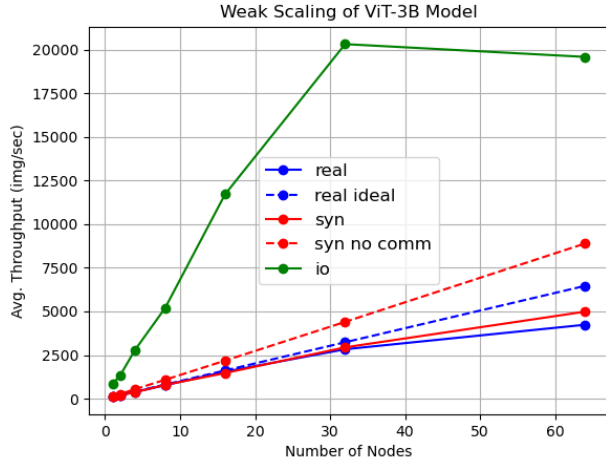


Fig. 1. Weak scaling plot of the MAE 3B parameter model. The solid blue line shows the measured average image-per-second (ips) of the real application, while the dash blue line (ideal) shows the ips drawn from an ideal linear scaling scenario without any additional costs as we scale. The "syn" plot, are runs on synthetic data, represent the compute and communication performance, while the "syn no comm" is synthetic on runs as well but without any communication. The "IO" plot shows the IO performance of the application. All hyper-parameters are kept constants for the tests, with a local batch-size 32 with "NO_SHARD" FSDP strategy.

Since it was shown the MAE workload is mostly compute and communication bound, for the rest of Section IV the performance runs are done on synthetic data as it will provide us with more insights of the performance. Moreover, as it was discussed in III-A, the ViT part of the MAE workload is the most compute-demand part and is the component of interest for model scaling, so we we are going to focus on the ViT architecture for the rest of the performance analysis.

B. Communication Optimizations with FSDP

In light of the insights from the previous sections, we investigate different FSDP sharding strategies to understand the trade-offs between compute and communication cost.

In addition to sharding options, FSDP provides several options for prefetching the parameters in the backward pass. In the *None* configuration, parameters for the next layer are requested after the communication calls between all FSDP ranks. In the *BACKWARD_POST* configuration the parameters are requested also before the communication calls but before the current layer drops its parameters, while the *BACKWARD_PRE* is even before the communication calls. Finally, FSDP also offers the *limit_all_gathers* option to synchronize the threads to prevent too many in-flight all-gathers.

Figure 2 shows the performance of three FSDP sharding strategies for the ViT-5B model for various configurations on eight nodes. Here we wanted to chose a model that can't fit on a single GPU, to highlight more possible differences in the configuration. Overall, we observe that *limit_all_gathers* option improves throughput for most configurations, with the highest gains observed for the *HYBRID_2GPUs* configuration. Moreover, the *BACKWARD_PRE* yields the highest throughput across most scenarios. This matches expectations since it provides the most overlap between compute and communication, although differences in performance are not very big. For the analysis that follows we fixed the parameters that provide us with the best image-per-second performance, i.e. *BACKWARD_PRE* and *limit_all_gathers*.

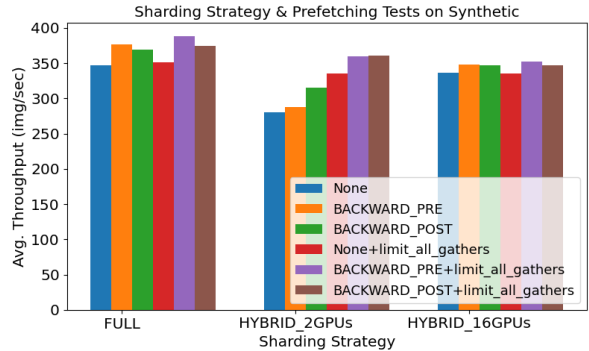


Fig. 2. Average image-per-second (ips) for the ViT-5B model architecture as a function of three sharding strategies for various FSDP configurations. All hyper-parameters are kept constants for the tests, with a local batch-size 32 on 8 Frontier nodes.

C. Weak scaling: ViT-Base to ViT-3B

Figure 3 shows the measured averaged image-per-second (ips) for the four ViT configurations of Table I that fit on a single GPU on Frontier. Here, we test the different sharding strategies explained in Section III against each other as well as against the well-established data-parallel (DDP) approach. We also evaluate the *HYBRID_1GPU* configuration, since although it should be equivalent with *NO_SHARD* (sharding-group is 1), their implementation PyTorch might differ and thus affect the communication and compute overlap.

The peak memory usage is also shown in Figure 3. The *HYBRID*, *DDP*, and *NO_SHARD* are constant as we use more nodes, while the *FULL_SHARD* shards parameters across all ranks, and so it depends on the number of GPUs used. We see the ViT-3B model uses more than 60 GB of memory per GPU, while when the model is sharded on two GPUs, i.e. *HYBRID_2GPUs*, the memory usage is dropped in half. For the *FULL_SHARD* we see a much bigger a drop in memory usage, up to 4 GB for the ViT-3B model, and this is expected since the model is sharded across all the available GPUs.

The weak scaling plots in Figure 3 show that the *FULL_SHARD* underperforms for all model sizes at scale. As we scale the model size the *FULL_SHARD* performs better as the number of nodes increases. For example, for ViT-B

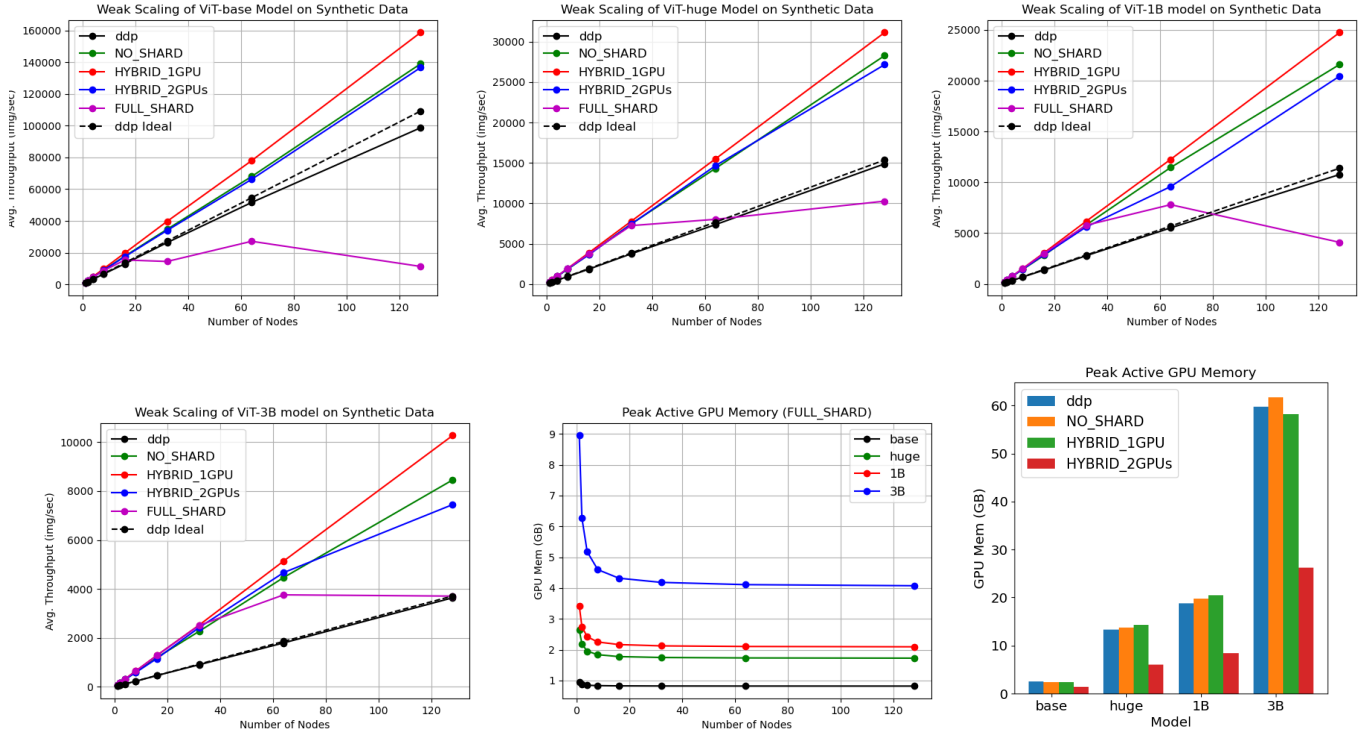


Fig. 3. The plots show the weak scaling for four model architectures: base (top left), huge (top center), 1B (top right) and 3B (bottom left). All four models can fit on a single GPU on Frontier. Also, the bottom center plot shows the memory usage of the FULL_SHARD mode, and the bottom right plot for the rest of the FSDP modes. The measured average image-per-second (ips) has been measured with a local batch-size of 32 for different FSDP sharding strategies as well as the distributed-data-parallel (DDP) strategy. The dash lines (ideal) show the ips drawn from an ideal linear scaling scenario without any additional costs as we scale. The memory usage per GPU for the DDP and HYBRID is constant, as we use more nodes, while the FULL sharding strategy is not.

the performance flattens for more than 16 nodes, while for ViT-3B it only flattens after increase to 64 nodes. So we can conclude for the FULL_SHARD strategy that when the compute is small, as we can see from the memory usage, the application becomes communication bound at a much smaller scale (as measured by number of workers) than compared to larger models with higher compute demands.

Figure 3 also shows that HYBRID_1GPU, HYBRID_2GPUs, and NO_SHARD are all faster than DDP. In terms of communication footprint, the NO_SHARD should be very similar to DDP, i.e. mostly all_reduce communication. However, the balance between the time the communication calls are issued and their message size matters a lot as we scale different model sizes. As we keep its default parameterization, DDP does keep a constant message size for the different models, which likely becomes too small as the model size increases. Meanwhile, FSDP in general seems to be better aware of the balance between communication call time and communication size, such that as we go from the ViT-base to the ViT-3B model the gap between DDP and FSDP grows larger. It is also interesting to note the compute and communication trade-offs: FULL_SHARD is faster at smaller scale compared to DDP, while the reverse holds as either the model size or the number of nodes increases.

Finally, another observation from Figure 3 is that HY-

BRID_1GPU performs better than HYBRID_2GPUs and NO_SHARD for all models. As shown by the memory footprint plots, the HYBRID_1GPU uses almost twice the memory of the HYBRID_2GPUs, which is expected since HYBRID_2GPUs shards the model parameters across the two closest GPUs. Yet, although the compute workload should be almost half for the HYBRID_2GPUs, the HYBRID_1GPU performs better for all model sizes. Most likely the reason is that the overhead for synchronization between the two GPUs, along with additional communication cost for model sharding, is bigger than the benefits of less compute workload. Also, we can see from the ViT-3B the difference between the two is even larger, compared with smaller models, indicating that the application is communication bound as we scale.

D. Sharding Strategies for Larger ViT Models

Figure 4 shows the measured image-per-second performance for different FSDP sharding strategies for two models that do not fit on a single GPU: ViT-5B and ViT-15B. The ViT-5B can fit on two GPUs using FSDP’s model sharding, while the ViT-15B can fit on four GPUs. We used a local batch size of 32 for both models, which represents a realistic workload for production runs.

For both models the FULL_SHARD method performs better as we scale, compared to Figure 3 where the ViT models

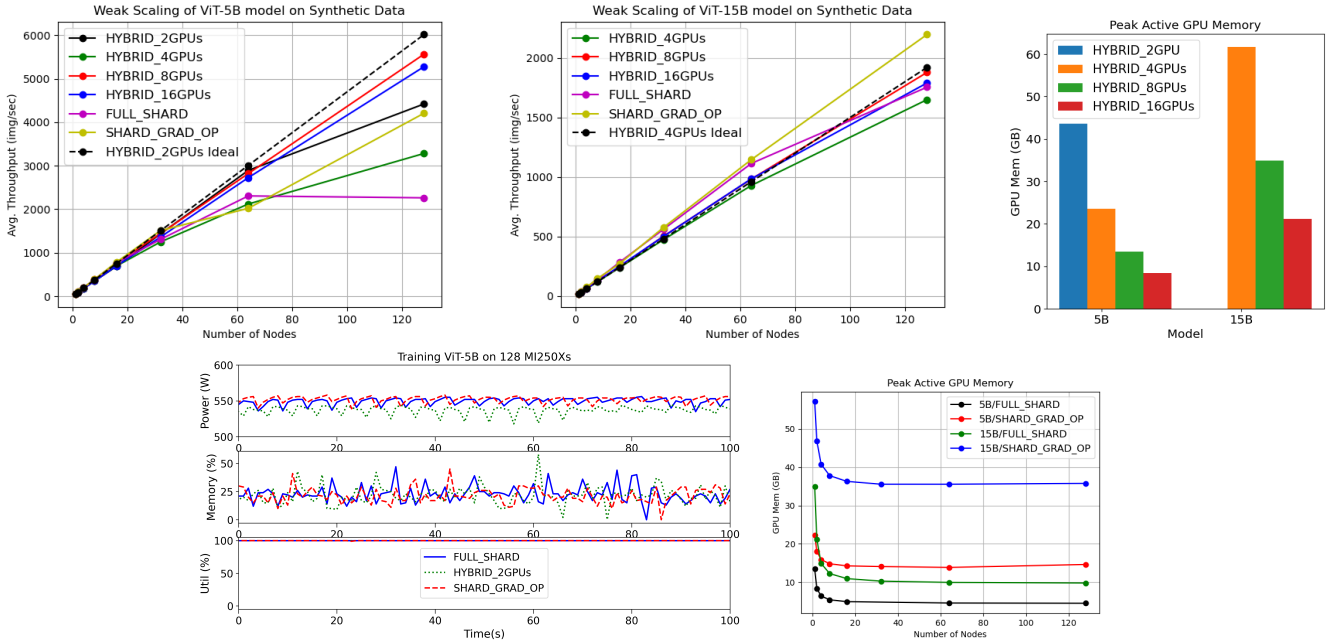


Fig. 4. The plots show the weak scaling of the 5B (top left), and 15B (top center) model architectures. The 5B does not fit on a single GPU on Frontier, while the 15B needs at least 4 GPUs to fit. Also, the top right and the bottom left plots show the memory usage of the HYBRID and FULL_SHARD FSDP modes respectively, for the two model architectures. The bottom left plot shows the GPU power, memory, and utilization trace for the different sharding strategies, on 32 node runs, for the 5B model using the *rocm-smi* utility. The average image-per-second (ips) is measured with a local batch-size of 32 for different FSDP sharding strategies. The dash lines (ideal) show the ips drawn from an ideal linear scaling scenario without any additional costs as we scale. The memory usage for HYBRID schemes is constant as we use more nodes, while the for FULL_SHARD and SHARD_GRAD it is not.

were able to fit on a single GPU. Interestingly, for the ViT-5B model the HYBRID_8GPUs and HYBRID_16GPUs seem to outperform the HYBRID_2GPUs and HYBRID_4GPUs strategies, despite the higher communication overhead expected of the former strategies as compared to the latter ones. The HYBRID_8GPUs and HYBRID_16GPUs configurations imply on larger numbers of communication calls, with all-gather operations passing through a slower network across nodes. Still, these results indicate that distributing the compute was more beneficial in this case in the trade-off with increased communication overhead.

For the ViT-15B model and its minimum configuration of HYBRID_4GPUs, we observe for the first time the FULL_SHARD and the SHARD_GRAD_OP modes being competitive with the HYBRID_SHARD modes. In fact, the SHARD_GRAD_OP configuration appears to scale significantly better than all other sharding strategies in this scenario. This further corroborates the observation made for the ViT-5B model that the compute load becomes the driving factor as compared to communication costs, which was in contrast the dominant factor for the smaller ViT models.

The memory footprint is also shown in Figure 4 for the two models. Since the SHARD_GRAD_OP does not share parameters during computation, but rather only gradients and optimizer states, its memory footprint is much larger than the FULL_SHARD configuration. However, compared to the FULL_SHARD, the SHARD_GRAD_OP shows a better bal-

ance between compute and communication for the ViT-15B experiments using Frontier. It is likely that if we scale the 15B to a much larger number of nodes, the SHARD_GRAD_OP would keep better performing than the FULL_SHARD, but at some point communication would potentially take over again and henceforth the HYBRID_SHARD modes would perform better than sharding across all ranks.

Finally, for a ViT-5B model the Figure 4 also presents the GPU power, memory, and utilization trace for the AMD GPUs for the different model sharding strategies. The GPU utilization is approximately 100%, which likely reflects the fact that we run on synthetic data and thus the interactions with CPU are minimum. Still, as we shown before, we are not IO bound in any of our runs. The SHARD_GRAD_OP implied on slightly higher power consumption compared to FULL_SHARD, which is consistent with the higher throughput that we get between the two (1509 versus 1307 image-per-second). It is noteworthy that the HYBRID_2GPUs, which is the most performing in terms of throughput (1509 ips), and likely the one with less communication calls compared to the other two, has the smallest power footprint.

E. Performance Observations

We first observed that as we scale the model size, the IO of the application is not a bottleneck, but rather communication cost is what drives the application performance. The BACKWARD_PRE and the *limit_all_gathers* seem to provide the best performance in terms of parameter prefetching. For

models that fit on a single GPU, the best data parallel strategy seems to be the HYBRID_1GPU, where the cost of synchronization even between the closest GPUs seems to be more expensive than the saves in the compute. It is worth noting that we did not try *torch.compile*, which can offer additional optimizations for overlapping compute and communication costs. For models that can fit on two GPUs, model sharding within the node and data parallel *all_reduce* across nodes seems to be the best choice. Finally, for models that can fit only on half of the Frontier node, the SHARD_GRAD_OP seems to scale better than any other FSDP mode.

V. DOWNSTREAM EVALUATION AS MODEL SCALES

In this section, we evaluate the performance of pretrained ViT-Base, ViT-Huge, ViT-1B and ViT-3B models for downstream adaptation on image classification datasets. Specifically, similar to [4] we first pretrain the models by pairing a MAE formulation with the 1M remote sensing images composing the MillionAID dataset [19]. We then perform linear probing of the four models for scene classification on three independent datasets.

Two main reasons are behind our choice for focusing on linear probing experiments rather than fine-tuning. First, linear probing implies on fewer task specific parameters and training, relying more strongly on the quality of the ideally generalizable features extracted by pretrained FMs. Moreover, fine-tuning results reported in the related literature for these datasets are nearly saturated (above 95% [3], [4]), such that any performance gains would be rather marginal and could potentially arise due to overfitting of a few wrong labels rather than providing insights on the quality of features being extracted by the pretrained models.

A. Datasets

Table II summarizes the four datasets used. The MillionAID dataset is one of the largest publicly available geospatial databases, with more than 1M million non-overlapping RS images spanning across 51 classes. Similar to related works [4], we used 990K images for pretraining and then randomly selected a total of 10K images across all categories for downstream adaptation and evaluation.

In addition to MillionAID, we followed [3] and [4] and assessed model downstream capabilities across the UC Merced Land Use (UCM) [26], the Aerial Image Dataset (AID) [27], and the NWPU-RESISC45 [28] collected by the Northwestern Polytechnical University.

B. Pretraining

In the following paragraphs, for shortness we adopt the prefix ViT to refer to our ViT models pretrained by means of MAE using MillionAID images (e.g., ViT-Base refers to a ViT-Base model pretrained through MAE). Our code is based on the original MAE work [16]. Figure 5 shows the pretraining loss for all four models, indicating lower training losses for the ViT-Huge, ViT-1B and ViT-3B models as compared to the ViT-Base. The hyper-parameters for all the models were kept

TABLE II
THE DIFFERENT DATASETS USED FOR PRETRAINING AND LINEAR-PROBING + EVALUATION ON DOWNSTREAM TASKS

Pretraining			
Datasets	Training Samples		
MillionAID	990848		

Image Classification			
Datasets	Training Samples	Testing Samples	Classes
MillionAID	1000	9000	51
UCM	1050	1050	21
AID	2000	8000	30
NWPU	3150	28350	45

identical for a fair comparison between them, with an input image size of 512×512 pixels, a base learning-rate of $1.5e-4$, and weight-decay of 0.05 with the AdamW optimizer. A global batch size of 2048 was used with the FSDP NO_SHARD strategy applied, with a local batch size of 32 and a 75% mask ratio of the original image used for all models.

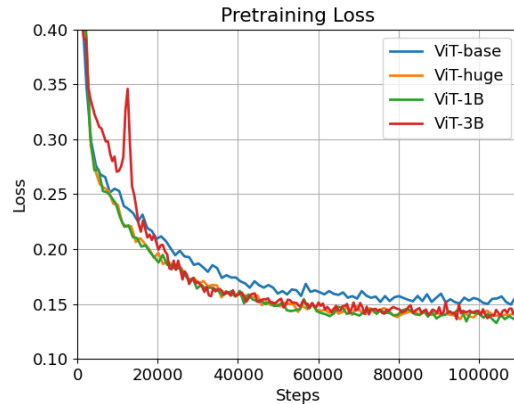


Fig. 5. The MAE pretraining loss of the four ViT models, base, huge, 1B, and 3B, as a function of steps, for an approximate total of 100 epochs.

C. Linear probing and image classification results

After the self-supervised pretraining, we used linear probing for downstream adaptation of the MAE-pretrained ViT models for image classification. Following common practice [16], the LARS [29] optimizer was used, with a base learning rate of 0.1 and no weight decay. The MLP heads of the model were replaced by a linear classifier for supervised training while keeping the weights for the rest of the model frozen. The hyper-parameters were kept identical for all models and datasets. A total number of 100 epochs was used for all the measurements. The global batch-size for UCM, AID and NWPU was kept identical with [4] at 256, while for the MillionAID dataset since there was no reference to compare, we chose 1024 for faster throughput.

We opt for pretraining our models for 100 epochs and fine-tuning for 100 epochs, in contrast to the 400 epochs of pretraining and 200 epochs of fine-tuning adopted for the ViT-Base models reported in [4]. Rather than pursuing an

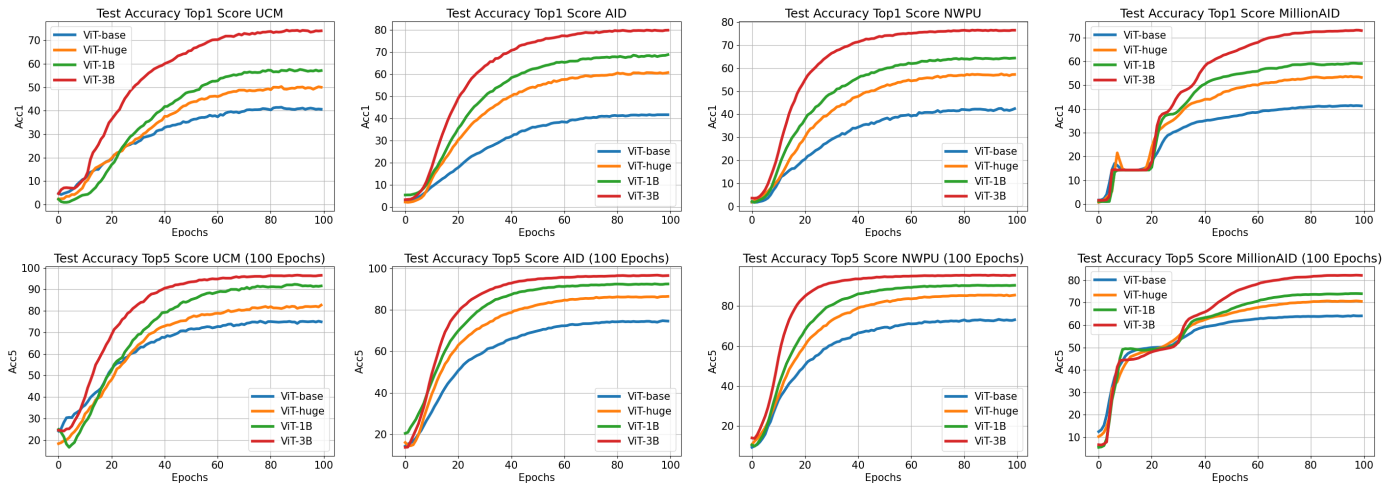


Fig. 6. The top1 and top5 classification accuracy, of the linear probe classification for the four MAE pretrained ViT models: base, huge, 1B and 3B for all testing datasets. The 100 epochs checkpoint was used from the pretraining, for each model architecture, while keeping all the hyper-parameters constant for the classification task. The training and testing dataset split is as shown in table II

indiscriminate use of computing resources and energy, we restrict the pretraining of our models as the results obtained already support the hypothesis that significant improvements are obtained as the models are scaled in size. Table III shows the top1 classification accuracy for the ViT-Base, ViT-Huge, ViT-1B and ViT-3B for all four image classification datasets.

TABLE III
LINEAR PROBING RESULTS ACROSS DIFFERENT RS IMAGE CLASSIFICATION DATASETS

Model	Pretrain epochs	Top1 Acc (%)			
		UCM (TR=55%)	AID (TR=28%)	NWPU (TR=19%)	MillionAID
ViT-Base [4]	400	49.90	61.70	61.28	

Model	Pretrain epochs	Top1 Acc (%)			
		UCM (TR=50%)	AID (TR=20%)	NWPU (TR=10%)	MillionAID
ViT-Base	400	45.17	52.11	54.28	47.20
ViT-Base	100	40.62	41.72	42.40	41.31
ViT-Huge	100	50.00	60.78	57.24	53.28
ViT-1B	100	57.10	68.89	64.35	59.14
ViT-3B	100	74.05	79.96	76.43	72.98

Importantly, results in Table III clearly reveal improvements in image classification performance as we scale the model size, for all four datasets evaluated. Remarkably, we observe more than 30% improvement across all four datasets when going from a 100M parameter to a 3B parameter model.

The differences in performance we observe between the ViT-Base reported in [4] and ours are most likely due to differences in data splits used for each dataset, as we adopt more rigorous training/test splits (i.e., fewer training samples). We denote TR the ratio of training samples used for each dataset: while we adopt $TR = 50\%$ for UCM, $TR = 20\%$ for AID and $TR = 10\%$ for NWPU, results in [4] were obtained with $TR = 55\%$ for UCM, $TR = 17\%$ for AID and $TR = 19\%$ for NWPU. Still, the pattern of performance

improvement as our models are scaled in size is evident, with results obtained by our ViT-Huge and larger models surpassing these numbers despite relying on fewer training samples and pretraining epochs.

Figure 6 expands the Table III by displaying the classification accuracy as a function of the number of linear probing training epochs, for the top1 and top5 classification accuracies. These curves reveal that top1 accuracy improvements become evident even as early as after 10 training epochs for UCM, AID and NWPU datasets, while the top5 accuracy follows a slower trend of improvement. In contrast, it is interesting to note how improvements for the MillionAID dataset occur rather later during training. The constant accuracy between 5 to 20 epochs, could possibly be improved by choosing a more aggressive learning rate decay, compared to the other datasets. Since MillionAID samples were also used for pretraining (but splitting between training and testing), the linear probing training samples in this case come from the same data-distribution as the pretraining samples. We conjecture this is the main factor explaining this difference with respect to the behavior observed for the other three datasets.

VI. CONCLUSION

Foundation models have emerged with desirable properties to integrate and synthesize vast amounts of knowledge toward new AI generalization capabilities. However, these models are yet to be fully explored and deployed in geospatial applications. This lag is due to multiple reasons: (i) these large models require vast HPC training resources that are not afforded to many in the community, (ii) the barrier of entry to training on HPC leadership facilities is high as the current hardware is very specialized and the expertise on effectively leveraging them remains restricted to few organizations, and (iii) pretraining billion-scale models on large RS data requires optimized strategies to data workflows. This study sought to address all three of these challenges and provide a practical

guide for training billion parameter size ViT models on HPC systems, using only native PyTorch’s distributed library. We provide baselines for various size ViT models, and discuss compute and communication costs to consider in training FMs for the largest geospatial application workloads to date. We also investigate the bottlenecks on distributing ViT training on the Frontier HPC system while scaling to various size models. Lastly, we evaluate our models via linear-probing and show gains up to +30% on remote sensing imagery classification tasks across three independent datasets. As much as we share new insights on training billion-scale FMs for RS, we also identify new research avenues that are worth following up in future research. Envisioned next steps include evaluation of model capabilities across additional downstream tasks (e.g., object detection and semantic segmentation), and under configurations such as few-shot learning to unveil potential properties emerging as we scale our models into multiple billions of parameters.

ACKNOWLEDGMENTS

A.T. would like to thank Less Wright from PyTorch team for the valuable discussions. This manuscript has been authored by UT-Battelle, LLC, under contract DE-AC05-00OR22725 with the US Department of Energy (DOE). The US government retains and the publisher, by accepting the article for publication, acknowledges that the US government retains a nonexclusive, paid-up, irrevocable, worldwide license to publish or reproduce the published form of this manuscript, or allow others to do so, for US government purposes. DOE will provide public access to these results of federally sponsored research in accordance with the DOE Public Access Plan (<http://energy.gov/downloads/doe-public-access-plan>). This research used resources of the Oak Ridge Leadership Computing Facility, which is a DOE Office of Science User Facility supported under Contract DE-AC05-00OR22725.

REFERENCES

- [1] Rishi Bommasani et al. On the opportunities and risks of foundation models. *arXiv preprint arXiv:2108.07258*, 2021.
- [2] Yezhen Cong, Samar Khanna, Chenlin Meng, Patrick Liu, Erik Rozi, Yutong He, Marshall Burke, David Lobell, and Stefano Ermon. Sat-mae: Pre-training transformers for temporal and multi-spectral satellite imagery. *Advances in Neural Information Processing Systems*, 35:197–211, 2022.
- [3] Xian Sun, Peijin Wang, Wanxuan Lu, Zicong Zhu, Xiaonan Lu, Qibin He, Junxi Li, Xuee Rong, Zhujun Yang, Hao Chang, et al. Ringmo: A remote sensing foundation model with masked image modeling. *IEEE Transactions on Geoscience and Remote Sensing*, 2022.
- [4] Di Wang, Qiming Zhang, Yufei Xu, Jing Zhang, Bo Du, Dacheng Tao, and Liangpei Zhang. Advancing plain vision transformer towards remote sensing foundation model, 2022.
- [5] Lu Yuan, Dongdong Chen, Yi-Ling Chen, Noel Codella, Xiyang Dai, Jianfeng Gao, Houdong Hu, Xuedong Huang, Boxin Li, Chunyuan Li, Ce Liu, Mengchen Liu, Zicheng Liu, Yumao Lu, Yu Shi, Lijuan Wang, Jianfeng Wang, Bin Xiao, Zhen Xiao, Jianwei Yang, Michael Zeng, Luwei Zhou, and Pengchuan Zhang. Florence: A New Foundation Model for Computer Vision, November 2021. arXiv:2111.11432 [cs].
- [6] Alec Radford, Jong Wook Kim, Chris Hallacy, Aditya Ramesh, Gabriel Goh, Sandhini Agarwal, Girish Sastry, Amanda Askell, Pamela Mishkin, Jack Clark, et al. Learning transferable visual models from natural language supervision. In *International Conference on Machine Learning*, pages 8748–8763. PMLR, 2021.

- [7] Chao Jia, Yinfei Yang, Ye Xia, Yi-Ting Chen, Zarana Parekh, Hieu Pham, Quoc Le, Yun-Hsuan Sung, Zhen Li, and Tom Duerig. Scaling up visual and vision-language representation learning with noisy text supervision. In *International conference on machine learning*, pages 4904–4916. PMLR, 2021.
- [8] Scott Reed, Konrad Zolna, Emilio Parisotto, Sergio Gomez Colmenarejo, Alexander Novikov, Gabriel Barth-Maron, Mai Gimenez, Yury Sulsky, Jackie Kay, Jost Tobias Springenberg, Tom Eccles, Jake Bruce, Ali Razavi, Ashley Edwards, Nicolas Heess, Yutian Chen, Raia Hadsell, Oriol Vinyals, Mahyar Bordbar, and Nando de Freitas. A generalist agent, 2022.
- [9] Olaf Ronneberger, Philipp Fischer, and Thomas Brox. U-net: Convolutional networks for biomedical image segmentation. In *Medical Image Computing and Computer-Assisted Intervention–MICCAI 2015: 18th International Conference, Munich, Germany, October 5–9, 2015, Proceedings, Part III 18*, pages 234–241. Springer, 2015.
- [10] Ashish Vaswani, Noam Shazeer, Niki Parmar, Jakob Uszkoreit, Llion Jones, Aidan N Gomez, Łukasz Kaiser, and Illia Polosukhin. Attention is all you need. *Advances in neural information processing systems*, 30, 2017.
- [11] Alexey Dosovitskiy, Lucas Beyer, Alexander Kolesnikov, Dirk Weissenborn, Xiaohua Zhai, Thomas Unterthiner, Mostafa Dehghani, Matthias Minderer, Georg Heigold, Sylvain Gelly, et al. An image is worth 16x16 words: Transformers for image recognition at scale. In *International Conference on Learning Representations*, 2020.
- [12] Xiaohua Zhai, Alexander Kolesnikov, Neil Houlsby, and Lucas Beyer. Scaling vision transformers. In *Proceedings of the IEEE/CVF Conference on Computer Vision and Pattern Recognition*, pages 12104–12113, 2022.
- [13] Mostafa Dehghani, Josip Djolonga, Basil Mustafa, Piotr Padlewski, Jonathan Heek, Justin Gilmer, Andreas Peter Steiner, Mathilde Caron, Robert Geirhos, Ibrahim Alabdulmohsin, et al. Scaling vision transformers to 22 billion parameters. In *International Conference on Machine Learning*, pages 7480–7512. PMLR, 2023.
- [14] Ting Chen, Simon Kornblith, Mohammad Norouzi, and Geoffrey Hinton. A simple framework for contrastive learning of visual representations. In *International conference on machine learning*, pages 1597–1607. PMLR, 2020.
- [15] Jacob Devlin, Ming-Wei Chang, Kenton Lee, and Kristina Toutanova. Bert: Pre-training of deep bidirectional transformers for language understanding. In *Proceedings of NAACL-HLT*, pages 4171–4186, 2019.
- [16] Kaiming He, Xinlei Chen, Saining Xie, Yanghao Li, Piotr Dollár, and Ross Girshick. Masked autoencoders are scalable vision learners. In *Proceedings of the IEEE/CVF Conference on Computer Vision and Pattern Recognition*, pages 16000–16009, 2022.
- [17] Kumar Ayush, Burak Uzket, Chenlin Meng, Kumar Tanmay, Marshall Burke, David Lobell, and Stefano Ermon. Geography-aware self-supervised learning. In *Proceedings of the IEEE/CVF International Conference on Computer Vision*, pages 10181–10190, 2021.
- [18] Gordon Christie, Neil Fendley, James Wilson, and Ryan Mukherjee. Functional map of the world. In *Proceedings of the IEEE Conference on Computer Vision and Pattern Recognition*, pages 6172–6180, 2018.
- [19] Yang Long, Gui-Song Xia, Shengyang Li, Wen Yang, Michael Ying Yang, Xiao Xiang Zhu, Liangpei Zhang, and Deren Li. On creating benchmark dataset for aerial image interpretation: Reviews, guidances, and million-aid. *IEEE Journal of selected topics in applied earth observations and remote sensing*, 14:4205–4230, 2021.
- [20] Lianmin Zheng, Zhuohan Li, Hao Zhang, Yonghao Zhuang, Zhifeng Chen, Yanping Huang, Yida Wang, Yuanzhong Xu, Danyang Zhuo, Joseph E Gonzalez, et al. Alpa: Automating inter-and intra-operator parallelism for distributed deep learning. *arXiv preprint arXiv:2201.12023*, 2022.
- [21] Yanli Zhao, Andrew Gu, Rohan Varma, Liang Luo, Chien-Chin Huang, Min Xu, Less Wright, Hamid Shojanazeri, Myle Ott, Sam Shleifer, Alban Desmaison, Can Balioglu, Pritam Damania, Bernard Nguyen, Geeta Chauhan, Yuchen Hao, Ajit Mathews, and Shen Li. Pytorch fsdp: Experiences on scaling fully sharded data parallel, 2023.
- [22] Jie Ren, Samyam Rajbhandari, Reza Yazdani Aminabadi, Olatunji Ruwase, Shuangyan Yang, Minjia Zhang, Dong Li, and Yuxiong He. {ZeRO-Offload}: Democratizing {Billion-Scale} model training. In *2021 USENIX Annual Technical Conference (USENIX ATC 21)*, pages 551–564, 2021.
- [23] Jeff Rasley, Samyam Rajbhandari, Olatunji Ruwase, and Yuxiong He. Deepspeed: System optimizations enable training deep learning models

with over 100 billion parameters. In *Proceedings of the 26th ACM SIGKDD International Conference on Knowledge Discovery & Data Mining*, KDD '20, page 3505–3506, New York, NY, USA, 2020. Association for Computing Machinery.

- [24] Alexey Dosovitskiy, Lucas Beyer, Alexander Kolesnikov, Dirk Weissenborn, Xiaohua Zhai, Thomas Unterthiner, Mostafa Dehghani, Matthias Minderer, Georg Heigold, Sylvain Gelly, Jakob Uszkoreit, and Neil Houlsby. An image is worth 16x16 words: Transformers for image recognition at scale, 2021.
- [25] The Frontier supercomputer. <https://www.olcf.ornl.gov/frontier/>.
- [26] Yi Yang and S. Newsam. Bag-of-visual-words and spatial extensions for land-use classification. In *ACM SIGSPATIAL International Workshop on Advances in Geographic Information Systems*, 2010.
- [27] Gui-Song Xia, Jingwen Hu, Fan Hu, Baoguang Shi, Xiang Bai, Yanfei Zhong, Liangpei Zhang, and Xiaoqiang Lu. Aid: A benchmark data set for performance evaluation of aerial scene classification. *IEEE Transactions on Geoscience and Remote Sensing*, 55(7):3965–3981, 2017.
- [28] Gong Cheng, Junwei Han, and Xiaoqiang Lu. Remote sensing image scene classification: Benchmark and state of the art. *Proceedings of the IEEE*, 105(10):1865–1883, 2017.
- [29] Yang You, Igor Gitman, and Boris Ginsburg. Large batch training of convolutional networks, 2017.